Optics Letters

Second- and third-order nonlinear wavelength conversion in an all-optically poled Si_3N_4 waveguide

Davide Grassani,[1,*] Martin H. P. Pfeiffer,[2] Tobias J. Kippenberg,[2] and Camille-Sophie Brès[1]

[1]Ecole Polytechnique Fédérale de Lausanne (EPFL), Photonic Systems Laboratory (PHOSL), Lausanne, Switzerland
[2]Ecole Polytechnique Fédérale de Lausanne (EPFL), Laboratory for Photonics and Quantum Measurements (LPQM), Lausanne, Switzerland
*Corresponding author: davide.grassani@epfl.ch

Received 14 September 2018; revised 14 November 2018; accepted 15 November 2018; posted 19 November 2018 (Doc. ID 345688); published 21 December 2018

Silicon nitride (Si_3N_4) is commonly employed to integrate third-order nonlinear optical processes on a chip. Its amorphous state, however, inhibits significant second-order nonlinear response. Recently, second-harmonic generation enhancement has been observed in Si_3N_4 waveguides after an all-optical poling (AOP) method. Here we demonstrate that, after AOP of a Si_3N_4 waveguide, for up to 2 W of coupled pump power, the same telecom-band signal undergoes larger interband wavelength conversion efficiency, based on sum-frequency generation (SFG), than intraband wavelength conversion, based on four-wave mixing. We also confirm the appearance of a phase-matching condition after AOP by measuring the conversion bandwidth and efficiency of SFG at different pump wavelengths.

https://doi.org/10.1364/OL.44.000106

Nonlinear wavelength conversion based on the Kerr effect in integrated photonic platforms enables high bandwidth (Tb/s) all-optical signal processing at the femtosecond time scale [1], optical amplification [2], and lasing [3], but also mid-infrared (IR) light generation [4–6] and emission of non-classical state of light [7–10]. Traditionally, silicon hosted most of these demonstrations because of its high nonlinearity and compatibility with complementary metal-oxide (CMOS) fabrication standards, which is highly desirable for combining optical and electronic capabilities on the same chip. Although exhibiting a lower nonlinearity than silicon, stochiometric silicon nitride (Si_3N_4) has been proposed for integrated nonlinear optical processes. In fact, it also offers compatibility with CMOS fabrication, and additionally features lower propagation losses and a very large transparency window, from the ultra-violet (UV) to the mid-IR. This avoids two-photon absorption, and consequently free-carrier absorption, which usually hampers silicon waveguides when pumped in the telecom band. Silicon nitride waveguides and resonators were then successfully employed for high-speed data conversion [11] and signal processing [12] in the telecom band, optical frequency combs [13], and supercontinuum generation [14,15]. Despite the large number of devices enabled by processes based on third-order optical nonlinearity ($\chi^{(3)}$), one of the major challenges in using materials compatible with CMOS technology is their lack of second-order nonlinearity ($\chi^{(2)}$) and, up to now, $\chi^{(2)}$ functionalities are mostly implemented off-chip in bulk crystals or periodically poled ferroelectric waveguides [16].

Recently, we reported [17] on the enhancement, of more than three orders of magnitude, of second-harmonic generation (SHG) in Si_3N_4 waveguides fabricated by low-pressure chemical vapor deposition (LPCVD). The enhancement appeared as a consequence of an all-optical poling (AOP) process, which consists of the irradiation of the waveguide with hundreds of picosecond-long pulses, which are then amplified up to a watt-level average power. Afterwards, analogous observations have been made independently using a near-IR mode-locked Yb-fiber laser with 6.2 ps of pulse duration in a very similar waveguide platform [18]. The phenomenon can be explained by the build-up with time of a static electric field (E_{DC}) along the waveguide, leading to an electric field induced SHG [19] in which an effective $\chi^{(2)}$ is generated through the $\chi^{(3)}$ of Si_3N_4 via the relation $\chi^{(2)} \approx E_{DC}\chi^{(3)}$. Similar to what has been reported for the SHG in silica optical fibers [20,21], the origin of the E_{DC} is assumed to be given by the charge trapping of electrons, excited by different multi-photon absorption processes from both the pump and second-harmonic waves, in defect states inside the Si_3N_4 bandgap. This process, known as the coherent photogalvanic effect [21], implies that the quantum interference among such different processes allows the E_{DC} to have the correct periodicity to quasi-phase match the SHG at the employed pump wavelength. To be triggered, AOP thus needs an initial SHG, which is usually present in Si_3N_4 waveguides as a consequence of a weak, native $\chi^{(2)}$ due to interface states or a non-zero average distribution of the Si-N dipoles. An initial second-harmonic seed can be generated if the phase-matching condition is fulfilled, i.e., the effective index of the pump mode equals the effective index of the second-harmonic mode. Considering the strong index dispersion of the waveguide on such a large spectral span, this condition

is usually achieved by intermodal phase-matching, where the second-harmonic is generated on a high-order mode.

Here we show interband wavelength conversion of a telecom band signal toward the near-IR via sum-frequency generation (SFG) in a Si_3N_4 waveguide that had been previously all-optically poled. We experimentally investigate the SFG conversion bandwidth and efficiency by probing the waveguide with a tunable continuous-wave (cw) laser. We confirm that, after AOP, the waveguide exhibits a defined phase-matching wavelength. Finally, we show how the interband conversion efficiency (CE) by SFG overcomes by at least one order of magnitude the intraband CE obtained by four-wave mixing (FWM) in the same waveguide. We estimate that FWM reaches the CE of SFG (at about −21.4 dB) for a coupled pump power of 2 W.

The waveguide under test consists of a Si_3N_4 core buried in a silicon dioxide (SiO_2) cladding. The waveguide is fabricated following the photonic Damascene process [22] and features a cross section of 1500×870 nm^2. The length is 40 mm, including inverse taper mode converters at both ends. Light is coupled into the waveguide with 5 dB insertion losses via a lensed fiber, while an objective is used for out-coupling with 6 dB of losses. Propagation losses are about 1 dB (0.25 dB/cm). After the objective, the collimated beam passes through a dichroic mirror with cutoff wavelength at 950 nm, providing about 20 dB of attenuation of the pump at the transmission port. We monitor the pump power at the reflecting port of the dichroic while SHG is detected with a silicon photodetector at the transmitting port, where we also employ an additional short-pass filter (cutoff wavelength at 1000 nm) to eliminate residual pump light, and a long-pass filter (cut-on wavelength at 600 nm) to filter out possible green light coming from third-harmonic generation.

First, we induce in the waveguide a $\chi^{(2)}$ grating via AOP. We modulated a telecom-band tunable fiber laser to obtain 1 ns long pulses with a repetition rate of 5 MHz. The pulses then passed through a two-stage erbium-doped fiber amplifier (EDFA) and a band-pass filter 1 nm in width centered at the pump wavelength, to eliminate pulse broadening due to self-phase modulation within the EDFA. Coupling the pump on the transverse-magnetic (TM) mode of the waveguide, an initial weak SHG triggers the AOP. Figure 1(a) shows that SHG grows about 25 dB over time when a constant pump power, measured at 34.5 dBm average at the chip input, is sent to the waveguide. A similar enhancement factor is extracted from the spectrum of the second-harmonic at the beginning and at the end of the process, reported in the inset in Fig. 1(a). Once the grating is induced and saturation is reached, we probe the waveguide in cw regime. In this case, the peak power coupled to the chip is much lower, and the SHG does not show any temporal signature. In Fig. 1(b), the estimated second-harmonic light generated inside the waveguide is shown as a function of the coupled cw pump power. The curve shows the expected quadratic dependence with a slightly slower slope at the highest power. Considering the large band-gap of Si_3N_4 and the employed power level, we attribute this to some possible misalignment of the in-coupling stage, rather than saturation due to multi-photon absorption. From this curve, we retrieve a CE for SHG of about 0.08%/W, which corresponds to a $\chi^{(2)}$ of about 0.65 pm/V if we consider the E_{DC} generated all over the length of the waveguide [17].

In order to test the signal conversion capabilities of the poled Si_3N_4 waveguide, we inject in the waveguide, through a 3 dB coupler, an additional telecom-band tunable cw signal. After the dichroic mirror, the remaining pump, SHG, and SFG are coupled into a multi-mode fiber through a parabolic mirror and sent to an optical spectrum analyzer. In this configuration, light at the pump and second-harmonic bands undergo, from the chip output to the detector of the spectrometer, about 30 dB and 10 dB of losses, respectively.

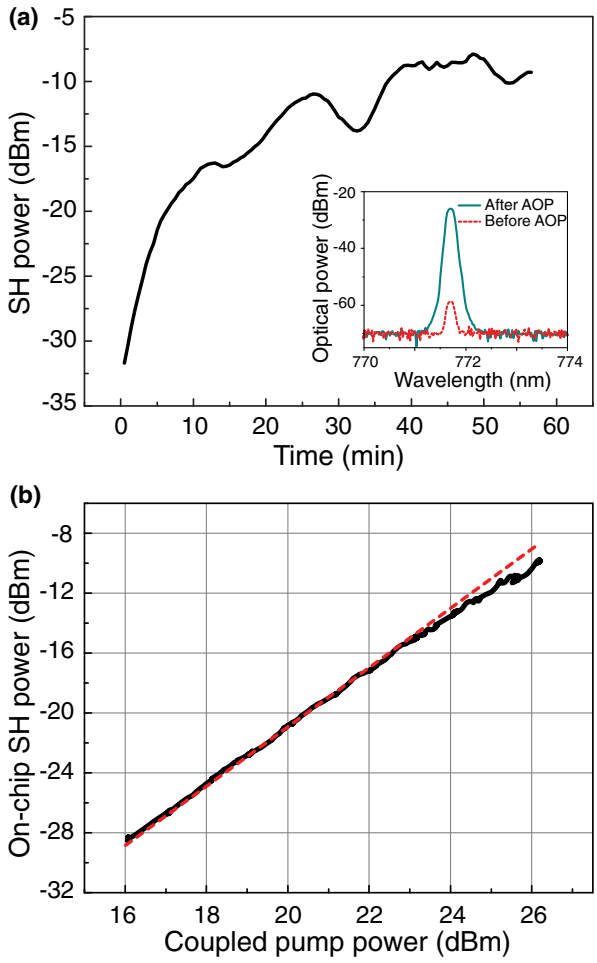

Fig. 1. (a) Second-harmonic generation enhancement over time at the detector during the all-optical poling process with a pump wavelength at 1543.5 nm. Inset: spectra of the second-harmonic of the pump source before and after the poling. (b) Estimated SHG inside the waveguide as a function of the pump power in cw regime. The red line represents a guide for the eye following a quadratic scaling.

Figure 2(a) shows an example of wavelength signal conversion within the pump band (intraband conversion), where an idler wave is generated by FWM at the wavelength $\lambda_i = \lambda_p\lambda_s/(2\lambda_s - \lambda_p)$. In addition to this $\chi^{(3)}$ process, and for the same coupled pump and signal powers, the waveguide clearly shows interband wavelength conversion from the pump to the SHG wavelength region [Fig. 2(b)]. Here, apart from the second-harmonic of the pump wave, we also observe that the signal is converted by SFG, a $\chi^{(2)}$ process, to a wavelength given by $\lambda_{SFG} = \lambda_p\lambda_s/(\lambda_s + \lambda_p)$. The conversion bandwidth for SFG is retrieved experimentally by sweeping the signal in wavelength. First, the pump is positioned at 1543.5 nm, the same wavelength used for the AOP. The results, plotted in Fig. 3(a),

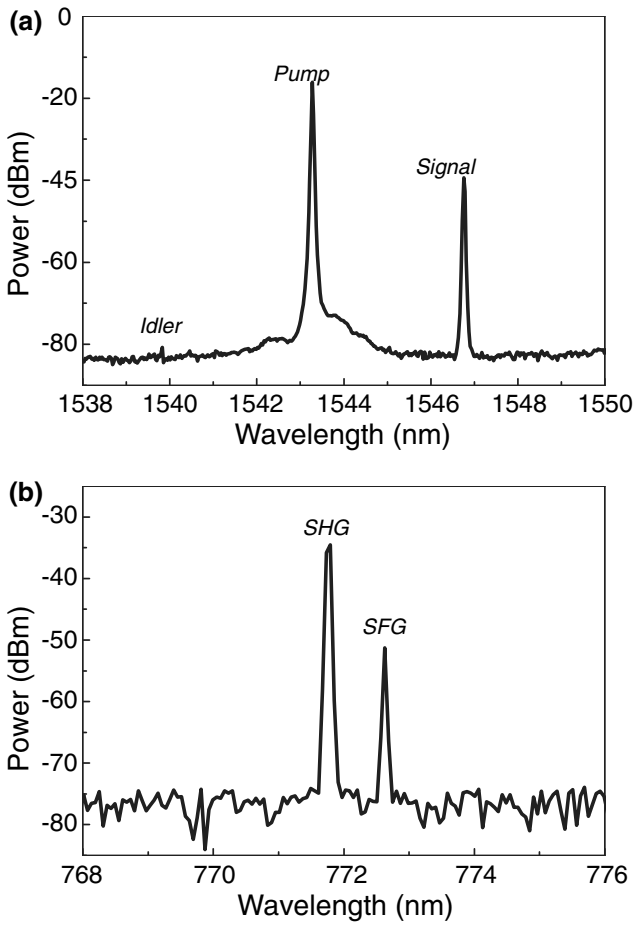

Fig. 2. (a) Example of FWM spectrum when 24 dBm of pump and 2 dBm of signal are coupled in the waveguide. (b) SFG spectrum with same pump and signal power and wavelength as in (a). The power levels of (b) are 20 dB larger then in (a) because of the disparity in the transmission of the dichroic mirror at the chip output.

clearly show that a maximum efficiency is reached when signal and pump lasers have the same wavelength. In this case, when the signal wavevector $\beta(\lambda_s)$ coincides with the pump wavevector $\beta(\lambda_p)$, the phase mismatch for SFG ($\Delta\beta_{\mathrm{SFG}} = \beta(\lambda_p) + \beta(\lambda_s) - \beta(\lambda_{\mathrm{SFG}})$) reduces to the phase mismatch for SHG ($\Delta\beta_{\mathrm{SFG}} = 2\beta(\lambda_p) - \beta(\lambda_p/2)$). The appearance of the maximum thus indicates that the phase mismatch is zero when $\beta(\lambda_s) = \beta(\lambda_p)$ and confirms that, after AOP, the waveguide can phase match the SHG of a laser placed at the poling wavelength [17]. The conversion spectrum is fitted with

$$P_{\mathrm{SFG}} = P_p P_s \left(\frac{2\omega_{\mathrm{SFG}} L \chi^{(2)} S}{\pi c n_{\mathrm{SFG}}}\right)^2 \left(\frac{\sin(\Delta\beta_{\mathrm{SFG}} L/2)}{\Delta\beta_{\mathrm{SFG}} L/2}\right)^2, \quad (1)$$

where L is the length of the $\chi^{(2)}$ grating and n_{SFG} the effective index of the SFG mode. The overlap integral S is obtained by simulating the waveguide dispersion and mode profiles with a finite-element-method-based software [17]. We assume both SHG and SFG to be on the same high-order TM waveguide mode characterized, before AOP, by the lowest phase mismatch with the pump on the fundamental mode. Clearly, the measured conversion bandwidth is larger than theoretically expected when considering $L = 40$ mm (green curve). This could suggest that a shorter grating of about 4 mm (blue curve) is actually inscribed in the waveguide, as recently reported also in Ref. [23]. In this case, $\chi^{(2)}$ would scale accordingly. However, other mechanisms which could be responsible for the broadening, notably phase fluctuation along the waveguide and involvement of multiple waveguide modes, are under investigation in our lab.

When changing the pump frequency from ω_p to $\omega_p' = \omega_p + \Delta\omega$, we do not expect to observe a change in the wavelength position of the maximum efficiency for SFG. In fact, imposing that phase-matching is always achieved when $\beta(\omega_p') + \beta(\omega_s) = 2\beta(\omega_p)$, and neglecting the effective index dispersion on the fundamental mode given that $\Delta\omega \ll \omega_p$, the optimal signal frequency is thus given by $\omega_s = \omega_p - \Delta\omega$. Therefore, SFG shows its maximum at $\omega_{\mathrm{SFG}} = \omega_p' + \omega_s = 2\omega_p$. In Figs. 3(b) and 3(c), we show the spectra obtained by sweeping the signal, for a pump wavelength at 1545 nm and 1548 nm, respectively. The results confirm that the phase-matching peak for SFG remains at the same position when changing the pump wavelength to 1545 nm. The small

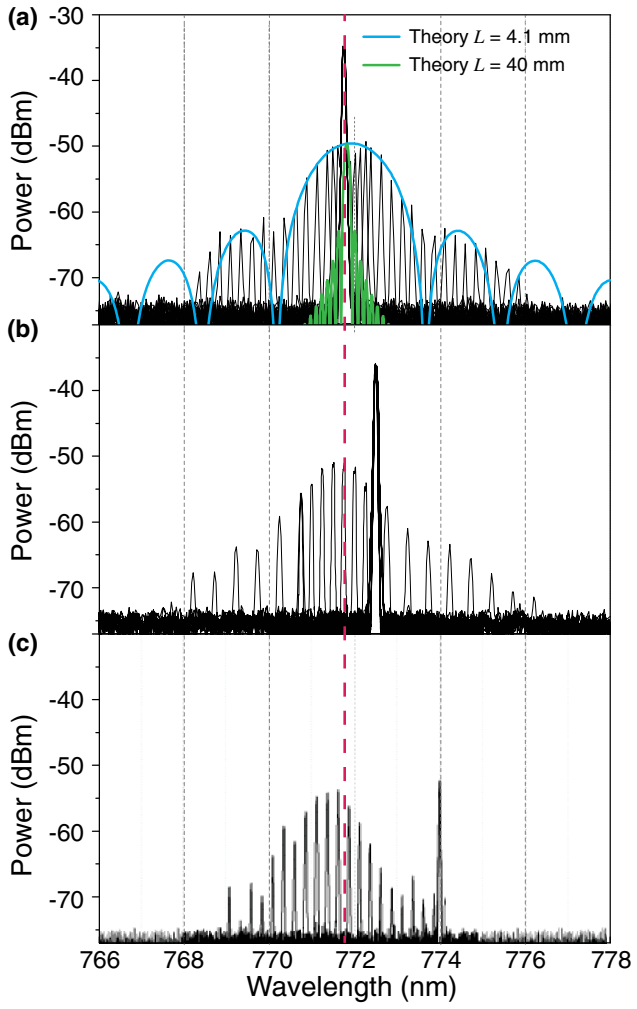

Fig. 3. SFG spectra sweeping the signal around the pump placed at (a) 1543.5 nm (poling wavelength), (b) 1545 nm, and (c) 1548 nm. Coupled pump and signal powers are 24 dBm and 2 dBm, respectively. Green (blue) curve: Eq. (1) considering sum-frequency generated in eighth TM mode; $L = 40$ mm (4.1 mm). The dashed red lines indicate maximum SFG for the pump at 1543.5 nm.

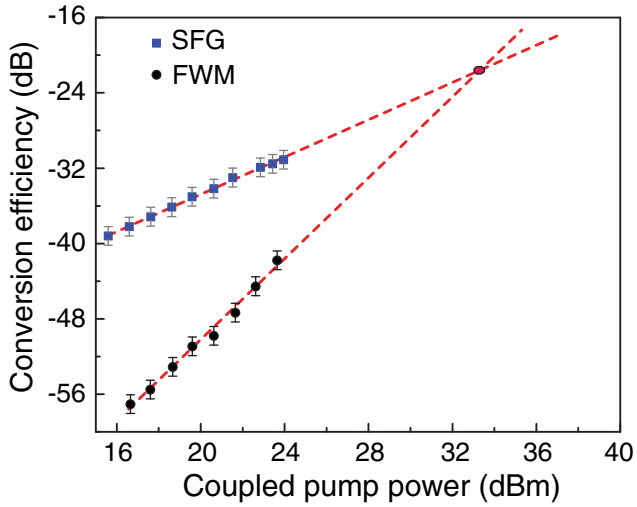

Fig. 4. SFG and FWM conversion efficiencies as a function of the pump power. The pump wavelength is at 1543.5 nm, while the signal is at 1543 nm. The red lines are the fit of the experimental points. The red dot represents the estimated parity point for the efficiencies of the two processes.

measured blue-shift for the longest pump wavelength [Fig. 3(c)] can be explained by considering that the larger is the shift ($\Delta\omega$) from the poling wavelength, the stronger is the contribution of the effective index dispersion. Figure 3 also shows that when the pump is red-shifted by 4.5 nm, SHG drops by 18 dB, but SFG stays within less than 3 dB variation, while the SFG conversion bandwidth does not clearly change.

Finally, we compare the CE of both FWM and SFG processes. We set the pump to the poling wavelength and the signal 0.5 nm away from the pump, such that the efficiency drop due to pump–signal phase mismatch can be neglected. In this configuration, we varied the pump power, keeping the signal power constant, and calculated the CE for FWM as the idler over signal power, and CE for SFG as SFG power over signal power. As seen in Fig. 4, both processes follow the correct power scaling as a function of pump power, namely, quadratic for FWM and linear for SFG. However, this result clearly shows that within the investigated pump powers, the interband signal CE, based on SFG, is at least 10 dB higher than the intraband FWM CE. From Fig. 4, we also estimate that the efficiency of FWM surpasses that of SFG for at least 2 W of pump power coupled to the waveguide. The $\chi^{(3)}$ we estimated from FWM is about 10^{-21} m^2/V^2, in agreement with what is reported for Si_3N_4 [24]. In principle, difference-frequency generation (DFG) between SHG and signal can produce a wave at the idler wavelength too. However, this cascaded second-order process scales with $(\chi^{(2)})^4$, and is at least two orders of magnitude lower than FWM, which scales with $(\chi^{(3)})^2$.

In conclusion, we have compared the efficiency of SFG and FWM for interband and intraband signal conversions in a Si_3N_4 waveguide that had been all-optically poled. We have confirmed the existence of a defined phase-matching condition for the $\chi^{(2)}$ process at the poling wavelength. This result shows that, although single-pass Si_3N_4 waveguides have been used mostly as a $\chi^{(3)}$ medium, while $\chi^{(2)}$ processes were evident by only employing resonant structures [25], the AOP method allows to efficiently integrate both $\chi^{(2)}$ and $\chi^{(3)}$ processes on the same CMOS-compatible photonic platform. This result can therefore potentially enable new photonic integrated functionalities, such as interband parametric amplification and oscillation, phase-only modulation, on-chip self-referencing of optical frequency combs, and generation of non-classical states of light.

Funding. H2020 European Research Council (ERC) (771647); Defense Advanced Research Projects Agency (DARPA) (HR0011-15-C-0055).

REFERENCES

1. J. Leuthold, C. Koos, and W. Freude, Nat. Photonics **4**, 535 (2010).
2. M. A. Foster, A. C. Turner, J. E. Sharping, B. S. Schmidt, M. Lipson, and A. L. Gaeta, Nature **441**, 960 (2006).
3. H. Rong, R. Jones, A. Liu, O. Cohen, D. Hak, A. Fang, and M. Paniccia, Nature **433**, 725 (2005).
4. X. Liu, R. M. R. Osgood, Y. Y. A. Vlasov, and W. M. J. W. Green, Nat. Photonics **4**, 557 (2010).
5. B. Kuyken, P. Verheyen, P. Tannouri, X. Liu, J. Van Campenhout, R. Baets, W. M. J. Green, and G. Roelkens, Opt. Lett. **39**, 1349 (2014).
6. S. Zlatanovic, J. S. Park, S. Moro, J. M. C. Boggio, I. B. Divliansky, N. Alic, S. Mookherjea, and S. Radic, Nat. Photonics **4**, 561 (2010).
7. S. Clemmen, K. Phan Huy, W. Bogaerts, R. G. Baets, P. Emplit, S. Massar, H. Rong, R. Jones, A. Liu, O. Cohen, and D. Hak, Opt. Express **17**, 16558 (2009).
8. S. Azzini, D. Grassani, M. Galli, L. C. Andreani, M. Sorel, M. J. Strain, L. G. Helt, J. E. Sipe, M. Liscidini, and D. Bajoni, Opt. Lett. **37**, 3807 (2012).
9. D. Grassani, S. Azzini, M. Liscidini, M. Galli, M. Strain, M. Sorel, J. Sipe, and D. Bajoni, Optica **2**, 88 (2015).
10. D. Grassani, A. Simbula, S. Pirotta, M. Galli, M. Menotti, N. Harris, T. Baehr-Jones, M. Hochberg, C. Galland, M. Liscidini, and D. Bajoni, Sci. Rep. **6**, 23564 (2016).
11. C. J. Krückel, V. Torres-Company, P. A. Andrekson, D. T. Spencer, J. F. Bauters, M. J. R. Heck, and J. E. Bowers, Opt. Lett. **40**, 875 (2015).
12. C. Lacava, S. Stankovic, A. Z. Khokhar, T. D. Bucio, F. Y. Gardes, G. T. Reed, D. J. Richardson, and P. Petropoulos, Sci. Rep. **7**, 22 (2017).
13. J. S. Levy, A. Gondarenko, M. A. Foster, A. C. Turner-Foster, A. L. Gaeta, and M. Lipson, Nat. Photonics **4**, 37 (2010).
14. A. S. Mayer, A. Klenner, A. R. Johnson, K. Luke, M. R. E. Lamont, Y. Okawachi, M. Lipson, A. L. Gaeta, and U. Keller, Opt. Express **23**, 15440 (2015).
15. H. Guo, C. Herkommer, A. Billat, D. Grassani, C. Zhang, M. Pfeiffer, W. Weng, C.-S. Brès, and T. Kippenberg, Nat. Photonics **12**, 330 (2018).
16. D. R. Carlson, D. D. Hickstein, A. Lind, S. Droste, D. Westly, N. Nader, I. Coddington, N. R. Newbury, K. Srinivasan, S. A. Diddams, and S. B. Papp, Opt. Lett. **42**, 2314 (2017).
17. A. Billat, D. Grassani, M. H. P. Pfeiffer, S. Kharitonov, T. J. Kippenberg, and C.-S. Brès, Nat. Commun. **8**, 1016 (2017).
18. M. A. G. Porcel, F. Schepers, E. A. P. Jorn, T. Hellwig, M. Hoekman, R. G. Eideman, P. J. M. Van Der Slot, C. J. Lee, R. Schmidt, R. Bratschitsch, F. Carsten, and K.-J. Boller, Opt. Express **25**, 1542 (2017).
19. O. A. Aktsipetrov, A. A. Fedyanin, E. D. Mishina, A. N. Rubtsov, C. W. V. Hasselt, M. A. C. Devillers, and T. Rasing, Phys. Rev. **54**, 1825 (1996).
20. U. Österberg and W. Margulis, Opt. Lett. **11**, 516 (1986).
21. D. Z. Anderson, V. Mizrahi, J. E. Sipe, and C. Ban, Opt. Lett. **16**, 796 (1991).
22. M. H. P. Pfeiffer, A. Kordts, V. Brasch, M. Zervas, M. Geiselmann, J. D. Jost, and T. J. Kippenberg, Optica **3**, 20 (2016).
23. D. D. Hickstein, D. R. Carlson, H. Mundoor, J. B. Khurgin, K. Srinivasan, D. Westly, A. Kowligy, I. Smalyukh, S. A. Diddams, and S. B. Papp, "Self-organized nonlinear gratings for ultrafast nanophotonics," arXiv:1806.07547v1 (2018).
24. K. Ikeda, R. E. Saperstein, N. Alic, and Y. Fainman, Opt. Express **16**, 12987 (2008).
25. S. Miller, K. Luke, Y. Okawachi, J. Cardenas, A. L. Gaeta, and M. Lipson, Opt. Express **22**, 26517 (2014).